Jpn. J. Appl. Phys. Vol. 31 (1992) pp. 2352–2358
Part 1, No. 8, August 1992

Effect of Fermi Level Motion on ESR and Optical Properties of $CuAlS_2$

Igor AKSENOV* and Katsuaki SATO**

Faculty of Technology, Tokyo University of Agriculture and Technology, Koganei, Tokyo 184

(Received April 21, 1992; accepted for publication June 20, 1992)

Optical absorption and electron spin resonance (ESR) spectra have been studied in as-grown, Cr-doped, and annealed in different atmospheres $CuAlS_2$ crystals. It has been found that the major influence on the optical and ESR properties of $CuAlS_2$ crystals, obtained by chemical vapour transport, arises from the transition ions Fe^{3+} and Cr^{2+}, which are present in the crystal lattice as residual impurities. Thermal treated crystals exhibit drastic changes in their absorption and ESR spectra depending on the annealing atmosphere, which is explained by the process of the Fermi level motion in the vicinity of the Fe^{2+}/Fe^{3+} and Cr^{+}/Cr^{2+} demarcation levels. The results obtained show that the valence states of Fe and Cr ions and their relative amounts in each valence state are controlled by the position of the Fermi level in the band gap of the host crystal, and are stoichiometry on dependent.

KEYWORDS: $CuAlS_2$ ternary semiconductor, iron and chromium transition ion impurities, optical absorption spectrum, ESR spectrum, Fermi level

§1. Introduction

$CuAlS_2$ ternary semiconductor is the widest band gap member of $A^1B^2C_2^6$-type chalcopyrite compounds which is expected to be a possible canditate for blue-to-ultraviolet light emitting device application, since it has a wide enough direct band gap,[1] a rather low melting point with a simple chalcopyrite phase,[2] and emits strong purple luminescence.[3] However, all as-grown $CuAlS_2$ crystals exhibit p-type conductivity with resistivities higher than 10^4 Ω-cm and hole mobilities lower than 3 cm^2/Vs.[4] Since the concentration of native defects in ternary compounds is expected to be high, a high resistivity implies that materials under consideration are highly compensated with the Fermi level position close to the center of the band gap. A defect whose energy is near the center of the band gap will gain or lose electrons as the Fermi level passes through the demarcation level of different charged (valence) states of this defect. The position of the Fermi level in the band gap can be influenced by appropriate thermal treatments of the crystal, and if any of the charged states of the defect are paramagnetic, the electron spin resonance (ESR) technique can be used to monitor the motion of the Fermi level in the vicinity of the demarcation level of the defect.

Transition atom (TA) impurities have been known to introduce deep levels in the band gaps of semiconductors, including the ternary ones, these levels not only taking part in the processes of electrical charge compensation and, therefore, controlling the concentration and type of conducting carriers, but also acting as activators or killers of luminescence.[5] The optical absorption and luminescence properties of ternaries depend greatly on the charged state of the TA impurities, which, therefore, can be determined from optical measurements. The concentration and type of residual impurities in ternary compounds depend greatly on the chemical purity of the starting materials, as well as on the technology used for material preparation.

It was shown by emission spectroscopy that contamination of $A^1B^3C_2^6$-type compounds occurs mainly by Fe and Cr,[6] whereas the ESR results show that the main contaminators are Fe and Ni, the valence states and the relative amounts of these elements in each valence state being stoichiometry on dependent.[7]

In this study we have tried to determine the type and valence states of TA impurities in the $CuAlS_2$ compound by 1) changing the position of the Fermi level in the band gap by stoichiometry alterations under thermal treatments in different atmospheres or by doping with donor- or acceptor-like impurities and by 2) controlling the resultant change in optical and ESR spectra.

§2. Experimental

The single crystals of the $CuAlS_2$ compound used in this study were as follows.

1) As-grown crystals of stoichiometric as well as Cu-rich ($Cu_{1.03}Al_{0.97}S_2$) and Al-rich ($Cu_{0.97}Al_{1.03}S_2$) compositions, grown by the temperature-variation chemical vapour transport (CVT) technique from the polycrystalline $CuAlS_2$ compound, prepared by the direct melting of constituent elements in a BN crucible.[8] Whereas most of the crystals, including those used for thermal treatments, were obtained from high-purity elements with the specified concentrations of Fe, Cr and Ni being less than 5 ppm, 2 ppm and 1 ppm, respectively, some of the as-grown crystals, used for optical absorption measurements, were prepared from starting elements contaminated with Fe and Cr in specified concentrations of 20 ppm and 50 ppm, respectively.

2) Cr-doped crystals with the nominal compositions $Cu_{0.98}Cr_{0.02}AlS_2$ and $CuAl_{0.98}Cr_{0.02}S_2$, obtained from the

*On leave from Institute of Physics of Solids and Semiconductors, Academy of Sciences of Buelorus, Minsk, Belorussia.
**To whom reprint requests should be addressed.

high-purity elements using the same growth method, Cr being added to the starting composition before melting. For the Cr-doped compound the CVT was carried out at two temperatures of the growth-zone, i.e., at the usually used $T_g=700°C$ as well as at higher $T_g=800°C$.

3) Crystals, annealed under vacuum, as well as in the presence of Cu and/or S. Thermal treatments were carried out in evacuated and sealed quartz ampoules with an inner diameter of 7–10 mm and 10–15 cm length. The samples were placed in one end of the ampoule and the annealing elements were placed in the other end. The thermal treatments were carried out for 60 h at 700°C (vacuum, S-, Cu-, Cu+S-annealings), as well as 750°C in the case of S-annealing, the amount of sulphur placed in the ampoule in the case of S-annealings corresponded to sulphur pressure of about 2, 4, and 6 atm at the temperatures used. Cooling down to room temperature was achieved by plunging the ampoule into water, and the sulphur stuck on the samples during the annealings in S-vapour was removed by washing the crystals in boiling CS_2.

Most of the as-grown single crystals were typically slightly greenish in colour and plate-shaped with dimensions of about $5\times10\times0.5\ mm^3$ or bulk-shaped with dimensions of $3\times3\times2\ mm^3$, whereas the Al-rich crystals were colourless with very small dimensions of no more than $5\times0.3\times0.2\ mm^3$. Annealing under vacuum yields colourless crystals, S-annealing deepens the blue-greenish colouration of the samples, and Cu- and (Cu+S)-annealings yield bright yellow crystals.

The crystals used for absorption measurements were mirror-polished to a thickness of 0.2–0.3 mm using lapping films. For ESR measurements relatively small plate-shaped or, better, bulk-shaped crystals were used. Absorption spectra were measured at room temperature using a HITACHI U-3410 spectrophotometer, and ESR spectra were taken with a JEOL JES-RE2X X-band spectrometer in the temperature range 110–300 K and microwave power range 0.01–150 mW. The crystals used for ESR measurements were not oriented by X-ray techniques, but we were able to ascertain the orientation of the crystals (at least, approximately) by comparison of the spectra obtained with those of the Ti- and V-doped crystals.[9]

§3. Results and Discussion

3.1 *Optical absorption*

3.1.1 *As-grown crystals*

The typical absorption spectra of undoped $CuAlS_2$ crystals are shown in Fig. 1. The spectrum of undoped nominally stoichiometric $CuAlS_2$ consists of two broad bands A and B at 920 and 620 nm, respectively, originating from charge-transfer transitions related to residual Fe^{3+} ions, substituting for Al sites.[10] Most of the crystals also exhibit a broad absorption C-band at ~1150 nm. The spectral position of the C-band agrees well with that of the Cr^{2+}-related absorption band in CdS:Cr,[11] where it was found to have originated from the intersystem transitions from the ground state $^5T_2$ of the Cr^{2+} ion to the excited states of $^3T_2$ and $^3T_1$ symmetry. However, if we assume that the C-band is caused by d-d transitions in divalent Cr ions, then we should also observe a strong absorption at ~1800 nm, originating from the intrasystem transitions $^5T_2\rightarrow{}^5E$.

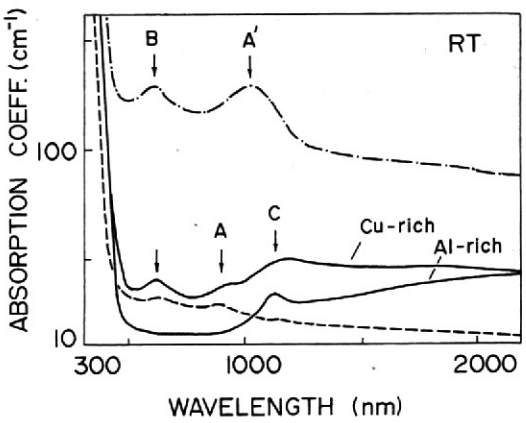

Fig. 1. Optical absorption spectra of the stoichiometric (----), Cu- and Al-rich (——) as-grown $CuAlS_2$ crystals, as well as of the crystals obtained from the starting elements contaminated with Fe and Cr in the specified concentrations of 20 ppm and 50 ppm, respectively (-·-·-).

Since no strong absorption band has been observed near 1800 nm in our crystals, the C-band may originate either 1) from Cr-related charge-transfer transitions or 2) from charge-transfer transitions from the valence band of the host crystal to the 3d-shell-originated orbitals of the Fe^{3+} ion, substituting for Cu sites. However, the latter assignment will be ruled out later on the basis of ESR results. Therefore, we tentatively attribute the C-band to Cr^{2+}-related charge-transfer transitions (the valence state of Cr ion has been determined from ESR results, discussed later).

The spectra of Cu-rich undoped crystals exhibit a slight increase in the intensities of A- and B-bands, whereas in Al-rich samples these Fe^{3+}-related bands are diminished or eliminated, the latter result being in accordance with that obtained by Donohue *et al.*[6] These results can be explained taking into account that in Cu-rich and Al-rich crystals a large concentration of the defects of antisite disorder should be expected, these defects being acceptor-like Cu_{Al}-defects for Cu-rich samples and donor-like Al_{Cu}-defects for Al-rich samples. These defects will influence the position of the Fermi level in the band gap of the host crystal, resulting in the change of valency of Fe ions, responsible for the A- and B-absorption bands.

The spectrum of the crystal, obtained from the starting elements, containing Fe and Cr impurities in high concentration (Fe ~ 20 ppm, Cr ~ 50 ppm), shows the great increase in absorption coefficient due to the strengthening of Fe and Cr-related absorption bands, the A-band in this case is shifted towards lower energies and labeled as A′.

3.1.2 *Cr-doped crystals*

The Cr-doped Cu-deficient crystals of the starting composition $Cu_{0.98}Cr_{0.02}AlS_2$, obtained by CVT at the growth-zone temperature $T_g=700°C$ exhibit no remarkable changes in the absorption spectrum as com-

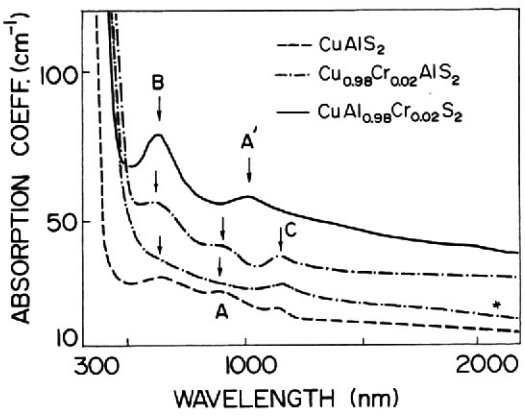

Fig. 2. Optical absorption spectra of Cr-doped $CuAlS_2$ crystals. The spectrum labeled by (*) belongs to the crystal obtained under a higher-than-usual temperature of the growth zone of the ampoule (T_g=800°C), used during CVT. The spectrum of undoped crystal is also shown.

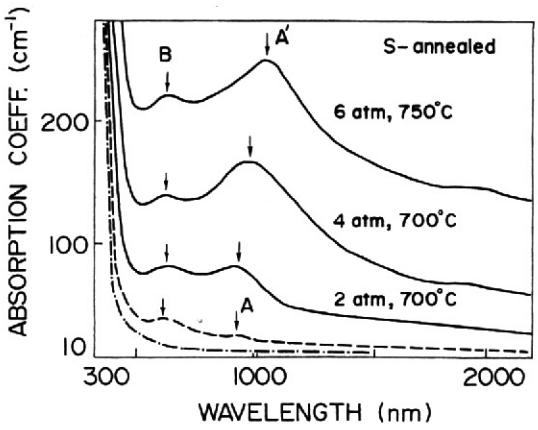

Fig. 3. Optical absorption spectra of S-annealed $CuAlS_2$ crystals. The spectra of undoped (----) and vacuum-annealed (-·-·-) crystals are also shown.

pared with the undoped stoichiometric crystals (Fig. 2), whereas increasing the T_g up to T_g=800°C results in elimination of the Fe^{3+}-related absorption bands in the crystals obtained, as shown by the curve marked by (*). The observed elimination of the Fe^{3+}-originated A- and B-bands can be explained under an assumption that in Cu-deficient crystals Cr ions tend to occupy Cu sites, since in this case the substitution of Cu^+ sites by either Cr^{2+} or Cr^{3+} leads to the reduction of Fe ions valency from Fe^{3+} to Fe^{2+} due to the upward shift of the Fermi level towards the conduction band. The same phenomenon has also been observed in V-doped $CuAlS_2$ crystals.[8] Since the above mentioned changes in the spectrum, witnessing the presence of Cr ions in the crystal lattice of host crystals, occurs only at high enough T_g, we believe that the transport rate of Cr during the CVT is slow and/or the probability of substitution of Cu sites by Cr is lower than that of Al sites.

The spectra of Al-deficient crystals, in which Cr is believed to substitute mainly for Al sites, exhibit the same A- and B-bands, but the peak energy of the A-band (9610 cm^{-1}) is shifted toward lower energies, the same "shifted" A'-band having been observed for our Fe- and Cr-contaminated samples (Fig. 1), as well as in the Cr-doped $CuAlS_2$, obtained by Donohue *et al.*[6] Therefore, the "shifted" A'-band is believed to be formed by both Fe^{3+}- and Cr^{2+}-related transitions, the Fe^{3+}-originated A-band and Cr^{2+}-originated C-band being superposed on each other and resulting in the A'-band.

3.1.3 *Annealed crystals*

The absorption spectra of S- and vacuum-annealed samples are shown in Fig. 3. It is seen from this figure that increasing the pressure of S as well as the temperature of the annealing results in an increase in intensity of the Fe^{3+}-related A- and B-bands, and in the shift of the A band towards its spectral position in the Cr-doped crystals (A'-band). Annealing of the crystals, previously annealed in S-vapour, in vacuum for 60 h results in a decrease in intensity of A'- and B-bands, whereas vacuum annealing for 120 h completely eliminates this transitions (Fig. 3) and results in colourless crystals.

The observed strengthening of the A- and B-bands as well as the shift of the A-band towards lower energies under S-annealing can be explained in terms of the Fermi level motion down toward the valence band of the host crystal. The thermal treatment in S-vapour will certainly result in a decrease of concentration of sulphur vacancies V_s, and in the increase of concentration of cation vacancies V_{Cu} and V_{Al}. Since the former defects are donor-like and the latter defects are acceptor-like, the degree of compensation under S-annealing will be reduced, which was observed experimentally as an increase of the conductivity of p-type samples.[4] The reduction of the degree of compensation means that the Fermi level in the samples moves from its midgap position in highly compensated crystals towards the valence band, this movement resulting in lowering of the Fermi level in relation to the demarcation levels of TA ions, i.e., Fe^{2+}/Fe^{3+} and Cr^+/Cr^{2+}, as compared with its position in as-grown samples. Therefore, both Fe and Cr ion impurities lose their electrons, this process resulting in the increase of concentration of Fe^{3+} and Cr^{2+} ions, which is observed as an increase of intensities of the absorption bands, originated from these ions, and in the decrease of the concentration of Fe^{2+} and Cr^+ ions.

For vacuum annealing the above-described processes are reversed, the Fermi level moving up towards the conduction band due to the increase in the concentration of V_s-defects, which results in the valency reduction of Fe and Cr ions to their optically undetectable states, Fe^{2+} and Cr^+. The formation of Cr^+ ions under vacuum annealing has been confirmed by ESR.

There are two more points that should be noted in connection with the observed absorption spectra of annealed crystals.

1) The annealing in Cu accelerates the process of the valency reduction of TA ions as compared with vacuum annealing. This is explained by the decrease in the concentration of acceptor-like V_{Cu}-defects, this process being superposed on the increase of concentration of V_s, which results in a "faster" upward movement of the Fermi level.

2) The thermal treatment in (Cu+S)-atmosphere does

not result in the strengthening of A- and B-bands, which was expected taking into account the much greater pressure of S as compared with that of Cu, but, to the contrary, it results in a decrease of the intensity of Fe-related absorptions. This result can be explained under an assumption that Cu diffuses readily through the chalcopyrite lattice, filling its vacancies, V_{Cu}, faster than S fills V_S, which results in the movement of the Fermi level upwards (not downward, as might have been expected under S-annealing). This assumption is supported by the low activation energy (0.5 eV) of Cu diffusion in binary sulphides.[12] The last result has also been confirmed by ESR.

3.2 *ESR*

3.2.1 *As-grown crystals*

The ESR spectra of undoped stoichiometric $CuAlS_2$ crystals at 110 K are shown in Fig. 4. The spectrum, taken under parallel orientation of the *c*-axis of the sample in relation to the external magnetic field H, consists of five fine structure transitions attributed to Fe^{3+} ions with $3d^5$ ($S=5/2$) electronic configuration.[13,14] Although in a perfect host lattice in a strong Zeeman effect approximation the peak-to-peak intensities of the five fine structure transitions of the Fe^{3+} ion should be in the ratio of 5:8:9:8:5, the peak amplitudes observed do not follow these ratios, presumably due to the effect of large crystal field splitting of the ground state of Fe^{3+} ions on Al sites, which will be discussed in detail later. The fine structure transitions are broadened up to the linewidths of about 8 mT for $\pm 3/2 \rightarrow \pm 1/2$ transitions and 15 mT for $\pm 5/2 \rightarrow \pm 3/2$ transitions, presumably due to the effects of random crystalline fields, unresolved hyperfine interaction with the nuclear moments of the ^{63}Cu and ^{27}Al nuclei, and spin-phonon interaction. Measurements, carried out in the range of microwave power from 0.01 mW to 150 mW, showed that microwave saturation for Fe^{3+}-related lines could not be reached even at the highest power used, which precluded any relaxation time estimations.

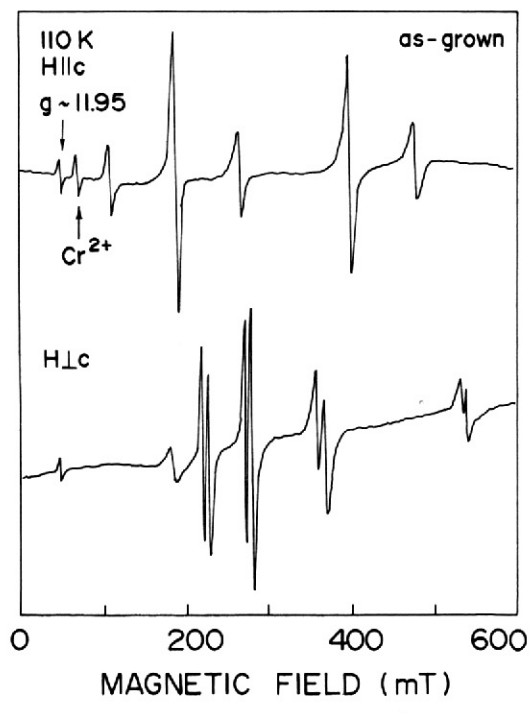

Fig. 4. ESR spectra of undoped nominally stoichiometric $CuAlS_2$ crystals.

In addition to the Fe-related transitions a nearly isotropic line at $g=11.95$ as well as an anisotropic line at $g_{//}=8.15$ were found to be present in undoped crystals. We cannot explain the nature of the line at $g=11.95$, since no lines with such a large *g*-value were observed in binary or ternary compounds. We can only say that this line must originate from some impurity or native defect, the ground state of which carries a very large amount of orbital momentum. On the other hand, the anisotropic line at $g_{//}=8.15$ can be readily assigned to the transitions within the lowest orbital singlet ground state of Cr^{2+} ion at substitutional sites of tetragonal symmetry, since the anisotropic Cr^{2+}-related lines with *g*-values, close to that observed in this study, have been found in binary compounds CdS[15] ($g_{//}=7.75$) and ZnSe[16] ($g_{//}=7.837$).

The spectrum of stoichiometric crystals, taken for the orientation $H \perp c$, exhibits the same fine structure of Fe^{3+} ions as well as the unidentified line at $g=11.95$, the fine structure lines being split into two components due to the presence of two magnetically unequivalent metal sites in the chalcopyrite lattice.[13] In this case the integral intensities of fine structure transitions approximately follow the ratio 5:8:9:8:5, the most intense $-1/2 \rightarrow +1/2$ transition being in the centre of the spectrum. However, we could not assign the fine structure transitions to the positive or negative spin values because the ESR spectra were recorded at relatively high temperatures. In the strong Zeeman field approximation the intensity ratio between two extreme transitions $3/2 \rightarrow 5/2$ and $-5/2 \rightarrow -3/2$ is nearly $\exp(-4h\nu/kT)$. In our case, taking into account the highest (300 K) and the lowest (110 K) temperatures used, this intensity ratio equals about 1.015, which, of course, is practically indiscernible in the spectrum.

The spectra of the Cu-rich crystals were practically the same as described above, whereas the spectra of the Al-rich samples exhibit a decrease of intensity of the Fe^{3+}- and Cr^{2+}-related lines, which is in accordance with the results of optical absorption, and the elimination of the unidentified line at $g=11.95$. In some Cu-rich samples, as well as in all the samples grown from contaminated starting elements, a broad line with *g*-values depending on orientation of the crystal and changing in the range of $g=2.05$–2.31, has also been found, this line being attributed to the transitions within the lowest Kramers doublet of the substitutional Ni^+ ion.[7,17] Moreover, the crystals grown from the contaminated starting elements have also exhibited a well-resolved 30-line ESR structure attributed to Mn^{2+} ions, since, for this ion with $3d^5$-configuration, the sixfold spin degeneracy results in five fine-structure lines, each of which is split into six hyperfine lines by the nuclear spin $I=5/2$ of ^{55}Mn.[18]

3.2.2 *Annealed and Cr-doped crystals*

The ESR spectra of the crystals annealed in S-vapour show no remarkable changes as compared with the spec-

tra of as-grown crystals, shown in Fig. 4, except that the intensities of the Cr^{2+}-related line and Fe^{3+}-related fine structure lines exhibit an approximately twofold increase. This result implies that most of the Fe and Cr ions in the lattice of the as-grown crystals are present in the form of Fe^{3+} and Cr^{2+}, which means that the Fermi level is shifted from the middle of the band gap toward the valence band.

On the other hand, the crystals annealed in Cu or in vacuum exhibit drastic changes in their ESR spectra (Fig. 5). In this case the spectra at room temperature show only one isotropic line at $g=1.998\pm0.005$ that exhibits the fine structure consisting of five components at temperatures below 220 K, which is shown in Fig. 5 for two orientations of the crystal. The observed structure has been assigned to the fine structure transitions of Cr^+ ions since 1) Cr^+ ions exhibit the isotropic g-value of 1.9995 in ZnS compound,[19] that is an isoelectronic analogue of $CuAlS_2$, and 2) the observed number of the components of fine structure agrees with the number of those that would be expected from an ion with $3d^5$-electronic configuration ($S=5/2$). The observed pattern is surely a fine structure, not hyperfine, because it is resolved up to temperatures of 220 K, and because the components of the structure are not equidistant, which would be expected for hyperfine interaction.

The observed elimination of Fe^{3+}- and Cr^{2+}-originated transitions and the appearance of Cr^+-related transitions in the ESR spectra of Cu- and vacuum-annealed crystals are in complete agreement with the results of optical absorption measurements, discussed in a previous paragraph in terms of the Fermi level motion in the band gap of the host crystal. However, while the conversion of Cr^{2+} into Cr^+ and vice versa has been ascertained by ESR results, the conversion of Fe^{3+} into Fe^{2+} may be regarded as an assumption since no ESR signal of Fe^{2+} ion has been detected in our experiments. Nevertheless, we believe that the last assumption is sufficiently grounded since there was very little chance for us to detect Fe^{2+} ions at the temperatures used due to the very weak intensity of the Fe^{2+}-related ESR signal even at $T=20$ K.[20]

The spectra of Cr-doped $CuAlS_2$ are shown in Fig. 6. The Cu-rich crystals exhibit the Fe^{3+}-originated fine structure lines as well as an unidentified line at $g=11.95$. At orientation close to $H/\!/c$ a Cr^{2+}-originated resonance line can also be observed, the spectrum being practically the same as for the undoped stoichiometric samples. However, the Al-rich crystals, in which Cr is believed to substitute Cu sites, shows the drastic decrease or the complete elimination of Fe^{3+}-related fine structure and the appearance of a broad isotropic line at $g=1.998$, arising from the Cr^+ ion. In the latter case the spectra are very similar to those observed for vacuum-annealed crystals (Fig. 5), and the results of ESR investigations agree well with the results of optical measurements. The results obtained for Cr-doped crystals can be consistenly explained by the Fermi level motion in the band gap of the crystals (§3.1), taking into account that the Cr^{2+}_{Cu}-defect is donor-like, while both Cr^{+}_{Al} and Cr^{2+}_{Al}-defects are acceptor-like.

3.2.3 *Fe^{3+}-originated fine structure*

The results obtained show that the ESR and optical absorption properties of undoped $CuAlS_2$ crystals are determined, to a large extent, by the Fe^{3+} impurity, this impurity also being the major cause of the colouration in $CuAlS_2$ crystals.[6] It should be noted in connection with the Fe^{3+} impurity that, although the Fe^{3+}-originated fine structure in the ESR spectra observed in this study is

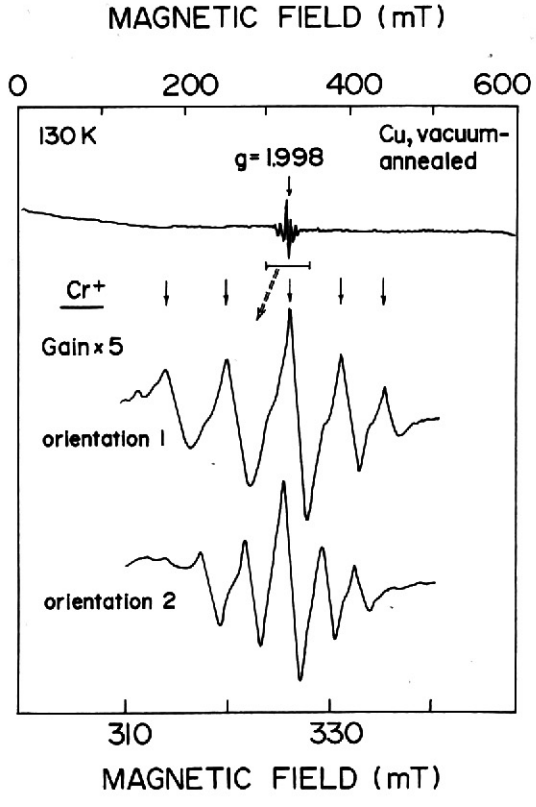

Fig. 5. ESR spectra of Cr^+ ion ($3d^5$-electronic configuration) in $CuAlS_2$ crystals, annealed in Cu and vacuum.

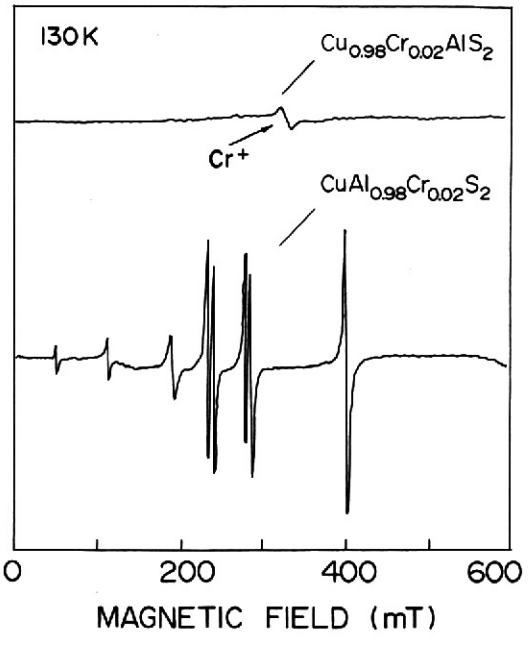

Fig. 6. ESR spectra of Cr-doped $CuAlS_2$ crystals at an arbitrary orientation.

similar to that observed previously in $CuXS_2$ compounds (X=Al, Ga, In),[13,14] the positions of all fine structure lines in our case are shifted towards lower values of the external magnetic field (i.e., to the higher g_{eff}-values) as compared with those previously reported.

If we take into account that not only the valency of Fe ions but also their positions in the lattice of the host crystal depend greatly on the technology of the material preparation, then the shift of the Fe^{3+}-originated fine structure can be explained under an assumption that Fe^{3+} ions in our crystals substitute for Al^{3+} sites, whereas in the crystals used by Brandt *et al.*[14] Fe^{3+} ions substitute for Cu^{+} sites. The substitution of Al site by Fe causes greater lattice distortion around the resulting defect compared with that in the case of Cu site substitution, since the ionic radius of Fe^{3+} (0.63 Å) is larger than that of the Al^{3+} ion (0.53 Å) but smaller as compared with Cu^{+} (0.74 Å). Moreover, the second shell ligands surrounding of the Fe_{Al}-defect is more covalent than that of the Fe_{Cu}-defect since in the former case each of the four sulphur anions surrounding the iron impurity forms bonds with two Cu cations (the Cu–S bonds being highly covalent) and one Al cation (the Al–S bonds being almost purely ionic), whereas in the latter case each S anion forms one bond with Cu and two bonds with Al.

The combined influence of the lattice strain and covalency can lower the symmetry around the substitutional defect, and results in a larger value of the cubic and axial components of the crystalline potential, usually used as terms in the spin Hamiltonian to describe the behaviour of ions with $3d^5$-electronic configuration with the orbital-singlet free-ion ground state $^6S_{5/2}$.

On excluding the hyperfine interaction arising from nuclei, the spectrum of Fe^{3+} can be analyzed in terms of the Hamiltonian[21]

$$\begin{aligned}\mathcal{H}=&g\beta HS+D[S_z^2-(1/3)S(S+1)]+(1/6)a\\&\times[S_\zeta^4+S_\eta^4+S_\delta^4-(1/5)S(S+1)(3S^2+3S-1)]\\&+(1/180)F[35S_z^4-30S(S+1)S_z^2+25S_z^2\\&-6S(S+1)+3S^2(S+1)^2],\end{aligned}\tag{1}$$

where a is the fourth-order cubic crystal field parameter responsible for the splitting of the highly symmetrical $^6S_{5/2}$-ground state in the cubic ligand field, D and F correspond to the axial fields of the second and fourth degree, and ζ, η, δ are the axes of the cubic crystalline fields.

For the strong-field Zeeman effect, when $g\beta H \gg a$, the spin Hamiltonian appropriate to the Fe^{3+} ion in tetragonal symmetry can be deduced from Hamiltonian (1) in the form[13]

$$\begin{aligned}\mathcal{H}=&g\beta HS+D(S_z^2-35/12)+(7/36)F[S_z^4\\&-(95/14)S_z^2+81/16]+(a/6)\\&\times[S_\zeta^4+S_\eta^4+S_\delta^4-707/16].\end{aligned}\tag{2}$$

Since Hamiltonian (2) has closed solutions for the magnetic field H directed along the z-axis (c-axis), it was used by Brandt *et al.*[14] to determine the values of $g_{/\!/}=2.020$, $D=900\times10^{-4}\,cm^{-1}$, and $a+(2/3)F=90\times10^{-4}\,cm^{-1}$ for Fe^{3+} ion in $CuAlS_2$ host, the value of g was determined directly from the position of the most intense line in the ESR spectrum, corresponding to $-1/2\rightarrow+1/2$ transition, by using the expression $g=h\nu/\beta H$. However, the last expression is only applicable when the terms of the order $a^2/g\beta H$ can be neglected, which seems to be true for Fe^{3+} ions on Cu sites, since the value of $a=60\times10^{-4}\,cm^{-1}$ in that case is small compared with the magnetic field of the resonance $g\beta H=11700\times10^{-4}\,cm^{-1}$.

However, in the case of Fe ions substituting for Al sites the large distortion of the lattice around the substitutional defect combined with the effect of covalency may cause an increase in the a, D, and E values, so that they (or one of them) will be comparable with the value of zero-field Zeeman splitting $g\beta H$. Since 1) our experimental results show that the magnetic field corresponding to the most intense $-1/2\rightarrow+1/2$ transition of the Fe^{3+} ion, varies with the orientation of the crystals from $H_{min}=190$ mT $(1770\times10^{-4}\,cm^{-1})$ to $H_{max}=400$ mT $(3730\times10^{-4}\,cm^{-1})$, and 2) an anomalously large value of the axial field term D $(4870\times10^{-4}\,cm^{-1})$ of the Fe^{3+} ion in $AgGaS_2$ host has been reported,[14] we suppose that in our case the substitution of Al sites by Fe ions causes ligand splitting, comparable with Zeeman splitting.

If Zeeman splitting is of the same order of magnitude as crystal field splitting, we can no longer use Hamiltonian (2), but have to deal with the general expression (1). Hamiltonian (1), except for the discussed above case of $g\beta H \gg a$, has only been solved for cubic symmetry for another limit case, i.e., when $g\beta H \ll a$.[22] It has been shown that in this case the Fe^{3+} free ion ground state is reduced to quadruplet and doublet states with the effective g-value for the lowest doublet being $(5/3)g_0=3.336$ (g_0 is the g-factor of a free electron) and the number of resonance lines in the spectrum being also five. Therefore, we suppose that Fe ions in our case substitute for Al sites, giving rise to the large crystal field splitting comparable with Zeeman splitting, caused by external magnetic field. Since there are no analytical solutions for Hamiltonian (1) in the case of $g\beta H \sim a$, D, we could not determine the g-value of the Fe^{3+} ion substituting for the Al site in the $CuAlS_2$ host.

§4. Energy Level Diagram

The observed changes in the ESR and optical absorption spectra of the $CuAlS_2$ crystals, caused by the thermal treatments in different atmospheres or by doping, can be explained taking into account the energy level diagram of $CuAlS_2$ (Fig. 7), in which the energy levels, formed by donor-like and acceptor-like native and extrinsic defects, as well as the position of the Fermi level in relation to the positions of the Fe^{2+}/Fe^{3+} and Cr^{+}/Cr^{2+} demarcation levels, are shown.

Since the as-grown $CuAlS_2$ crystals usually exhibit p-type conductivity with high resistivity values, we believe that in the as-grown crystals the Fermi level is shifted down a little from the midgap position, the Fermi level being lower than both Fe^{2+}/Fe^{3+} and Cr^{+}/Cr^{2+} demarcation levels. Therefore, in the as-grown crystals Fe^{3+}- and Cr^{2+}-related signals should be observed in optical absorption and ESR spectra, which is in good agreement with the experimental results.

Table I. The effect of the thermal treatments and doping on the optical and ESR spectra of $CuAlS_2$ crystals.

Treatment	Defects	Fermi level motion	Observed changes in the spectra		
			Fe^{3+}	Cr^{2+}	Cr^{+}
as-grown: stoichiometric		●	+	+	0
Cu-rich	$Cu_{Al}\uparrow$	↓▲	↑	↑	0
Al-rich	$Al_{Cu}\uparrow$	↑■	↓	↓	0
Cr-doped:					
Al-deficient	$Cr_{Al}\uparrow$	↓▲	↑	↑	0
Cu-deficient	$Cr_{Cu}\uparrow$	↑■	↓	+	↑
S-annealed	$V_S\downarrow$, $V_{cat}\uparrow$	↓△	↑	↑	0
Cu-, vacuum-annealed	$V_S\uparrow$	↑○	0	0	↑

+ no changes in the spectra compared with as-grown samples, the signal is detected;
0 the signal is not detected by optical absorption and ESR;
↑(↓) increase (decrease) of the concentration of defects or the intensity of the signal;
●, ▲, ■, △, ○ the resultant positions of the Fermi level, which are shown in Fig. 7.

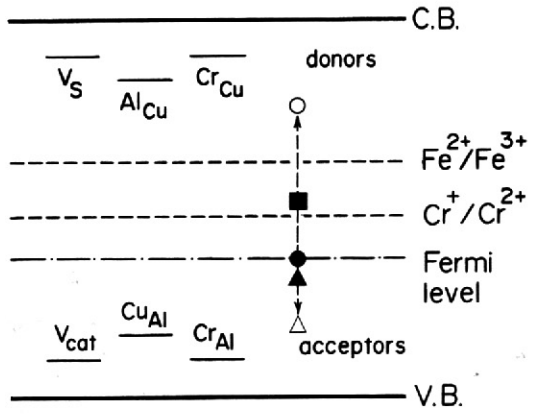

Fig. 7. A schematic energy level diagram of $CuAlS_2$:Fe, Cr. The positions of the donor- and acceptor-like energy levels are only schematic.

Doping and thermal treatments lead to a change in the concentration of donor- and acceptor-like defects, this change causing the shift of the Fermi level in relation to the TA-ion demarcation levels. The defects, responsible for the change in the degree of compensation of $CuAlS_2$ under annealings and doping, and the expected shift of the Fermi level, as well as the experimentally observed change in the optical absorption and ESR spectra of the crystals, are shown in Table I. It can be seen from Table I and Fig. 7 that the observed changes in the spectra are in good agreement with those that expected as a result of the Fermi level motion.

§5. Conclusions

In conclusion, the experimental results obtained in this study show that the major influence on optical and ESR properties of $CuAlS_2$ crystals arises from Fe and Cr transition ion impurities. The valence states of Fe and Cr ions and their relative concentrations in each valence state are controlled by the position of the Fermi level in the band gap of the host crystal in relation to the Fe^{2+}/Fe^{3+} and Cr^{+}/Cr^{2+} demarcation levels, this position being dependent on the concentrations of electrically active native and extrinsic defects, including the substitutional defects, formed by the said Fe and Cr ions.

The exact positions of the demarcation levels of Fe and Cr impurities can be determined using a photostimulated ESR technique since the trapping of electons and holes, produced by irradiation, by the Fe- and Cr-originated traps, can give us direct information about the energy separation between the demarcation levels of these ions and the valence band. This has not been attempted so far and is planned for the near future.

Acknowledgments

This study has been partially supported by the Japan Society for the Promotion of Science and by a Grant-in-Aid for Scientific Research from the Ministry of Education, Science and Culture, which is deeply appreciated.

References

1) J. L. Shay and J. H. Wernick: *Ternary Chalcopyrite Semiconductors: Growth, Electronic Properties, and Application* (Pergamon, Oxford, 1975) p. 118.
2) I. Aksenov, L. Makovetskaya, G. Popelnyuk and I. Shilovich: Phys. Status Solidi a **105** (1988) K97.
3) N. Yamamoto: *Proc. 4th Int. Conf. Ternary & Multinary Compounds, Tokyo, 1980*, Jpn. J. Appl. Phys. **19** (1980) Suppl. 3, p. 95.
4) I. Aksenov, I. Gulakov, V. Lipnitskii, A. Lukomskii and L. Makovetskaya: Phys. Status Solidi a **115** (1989) K113.
5) K. Sato, H. Tsunoda and T. Teranishi: *Proc. 7th Int. Conf. Ternary & Multinary Compounds, Snowmass, CO., 1986* (Mater. Res. Soc., Pittsburgh, 1987) p. 459.
6) P. C. Donohue, J. D. Bierlein, J. E. Hanlon and H. S. Jarrett: J. Electrochem. Soc. **121** (1974) 829.
7) H. J. von Bardeleben, A. Goltzene and C. Schwab: *Proc. 2nd Int. Conf. Ternary & Multinary Compounds, Strasbourg, 1975*, J. Phys. (France) **36** (1975) Suppl. 9, C3, p. 47.
8) I. Aksenov, Y. Kudo and K. Sato: Jpn. J. Appl. Phys. **31** (1992) L145.
9) I. Aksenov and K. Sato: Jpn. J. Appl. Phys. **31** (1992) L527.
10) K. Kondo, T. Teranishi and K. Sato: J. Phys. Soc. Jpn. **36** (1974) 311.
11) R. Pappalardo and R. E. Dietz: Phys. Rev. **123** (1961) 1188.
12) M. Aven and R. E. Halsted: Phys. Rev. A **137** (1961) 228.
13) J. Schneider, A. Räuber and G. Brandt: J. Phys. & Chem. Solids **34** (1973) 443.
14) G. Brandt, A. Räuber and J. Schneider: Solid State Commun. **12** (1973) 481.
15) K. Morigaki: J. Phys. Soc. Jpn. **19** (1964) 187.
16) M. de Wit, A. R. Reinberg, W. C. Holton and T. L. Estle: Bull. Am. Phys. Soc. **10** (1965) 329.
17) U. Kaufmann: Solid State Commun. **19** (1976) 213.
18) G. L. Troeger, R. N. Rogers and H. M. Kasper: J. Phys. C **9** (1976) L73.
19) R. S. Title: Phys. Rev. **131** (1963) 623.
20) U. Kaufmann: Solid State Commun. **19** (1976) 213.
21) B. Bleaney and R. S. Treham: Proc. R. Soc. London Ser. A **223** (1954) 1.
22) A. Abragam and B. Bleaney: *Electron Paramagnetic Resonance of Transition Ions* (Dover, New York, 1986) p. 144.